Cell Reports

Resource

Mapping functional elements of the DNA damage response through base editor screens

Graphical abstract

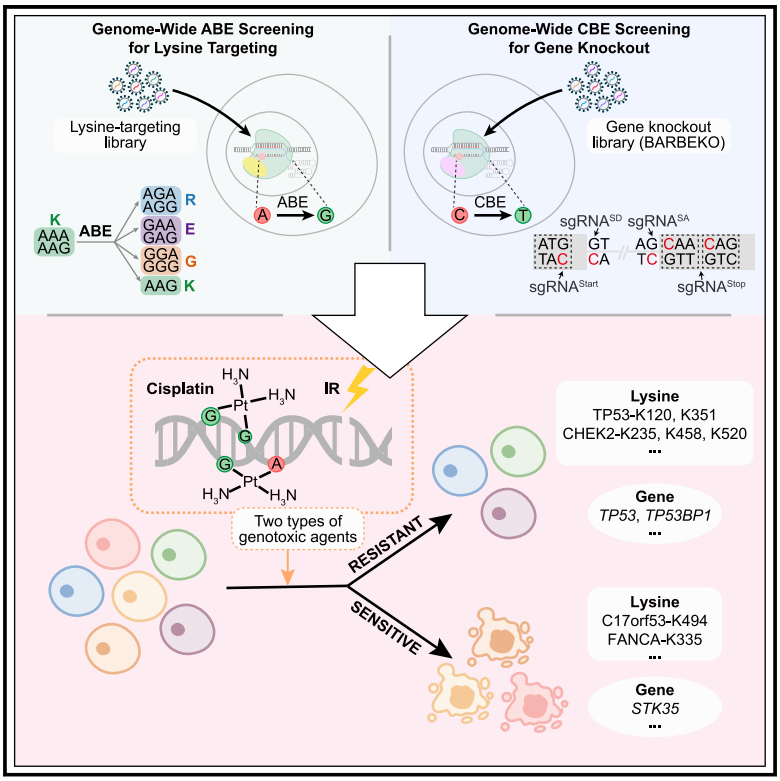

Authors

Qian Pan, Zhixuan Zhang, Yangfang Xiong, ..., Ying Yu, Zhuo Zhou, Wensheng Wei

Correspondence

wswei@pku.edu.cn

In brief

Pan et al. employ CRISPR-mediated base editing in pooled screens to investigate the functional lysine residues and genes affecting the DNA damage response. They identify the K494 mutation in C17orf53, which increases cisplatin sensitivity, and emphasize *STK35* as a novel gene involved in DNA repair, offering insights for cancer therapy.

Highlights

- Genome-wide screens of functional lysine residues and genes in DNA damage response
- Identification of known loss-of-function variants in *TP53* and *CHEK2*
- Increased sensitivity to cisplatin conferred by the K494 mutation in C17orf53
- STK35 as a candidate modulator of DNA damage response

Pan et al., 2024, Cell Reports *43*, 115047
December 24, 2024
https://doi.org/10.1016/j.celrep.2024.115047

CellPress

Cell Reports

CellPress
OPEN ACCESS

Resource

Mapping functional elements of the DNA damage response through base editor screens

Qian Pan,[1,4] Zhixuan Zhang,[1,4] Yangfang Xiong,[1] Ying Bao,[1,2] Tianxin Chen,[1] Ping Xu,[1] Zhiheng Liu,[1] Huazheng Ma,[1] Ying Yu,[1] Zhuo Zhou,[1,3] and Wensheng Wei[1,2,5,*]

[1]Biomedical Pioneering Innovation Center, Beijing Advanced Innovation Center for Genomics, Peking–Tsinghua Center for Life Sciences, Peking University Genome Editing Research Center, State Key Laboratory of Protein and Plant Gene Research, School of Life Sciences, Peking University, Beijing 100871, China

[2]Changping Laboratory, Beijing 102206, China

[3]State Key Laboratory of Common Mechanism Research for Major Diseases, Suzhou Institute of Systems Medicine, Chinese Academy of Medical Sciences & Peking Union Medical College, Suzhou 215123, Jiangsu, China

[4]These authors contributed equally

[5]Lead contact

*Correspondence: wswei@pku.edu.cn

https://doi.org/10.1016/j.celrep.2024.115047

SUMMARY

Maintaining genomic stability is vital for cellular equilibrium. In this study, we combined CRISPR-mediated base editing with pooled screening technologies to identify numerous mutations in lysine residues and protein-coding genes. The loss of these lysine residues and genes resulted in either sensitivity or resistance to DNA-damaging agents. Among the identified variants, we characterized both loss-of-function and gain-of-function mutations in response to DNA damage. Notably, we discovered that the K494 mutation of C17orf53 disrupts its interaction with RPA proteins, leading to increased sensitivity to cisplatin. Additionally, our analysis identified *STK35* as a previously unrecognized gene involved in DNA damage response (DDR) pathways, suggesting that it may play a critical role in DNA repair. We believe that this resource will offer valuable insights into the broader functions of DNA damage response genes and accelerate research on variants relevant to cancer therapy.

INTRODUCTION

Maintaining genome stability is vital for proper cellular function. DNA damage can arise from diverse factors, including external physical, chemical, and biological agents, such as viruses. To safeguard genomic integrity, cells employ various DNA repair pathways, including base excision repair, nucleotide excision repair (NER), mismatch repair, single-strand break repair, homologous recombination (HR), non-homologous end joining, and microhomology-mediated end joining.[1–7] Some types of DNA lesions require the coordinated action of multiple DNA repair pathways.

Post-translational modifications (PTMs) of proteins also play a critical role in the DNA damage responses,[8,9] although several PTMs remain poorly understood.[10] One example is the ataxia telangiectasia mutated (ATM)-CHK2 signaling cascade.[11] Studies have indicated that PTMs such as SUMOylation, ubiquitination, and glycosylation can interact with each other following DNA damage.[12,13] Lysine residues play a crucial role in this context because they act as key sites for various PTMs, such as ubiquitination and acetylation, which are essential for modulating protein function and stability.

Tumor cells exhibit increased sensitivity to DNA damage compared to normal cells because of their hyper-replication features.[14,15] This heightened sensitivity underpins the widespread use of radiotherapy and chemotherapy in clinical settings.[16] While effective, these treatments can cause dose-limiting toxicity in normal cells. Cisplatin, a key chemotherapeutic agent, induces interstrand DNA cross-links,[16–18] while radiotherapy utilizes ionizing radiation (IR), resulting in random single or double-strand DNA breaks.[19–21] However, many cancer patients develop drug resistance, frequently linked to mutations in DNA repair-related genes, with *TP53* being a prominent example.[22] Certain gene mutations may increase drug sensitivity,[23] emphasizing the importance of studying these mutations in the context of precision medicine.

Despite extensive research on genome maintenance mechanisms, critical DNA repair factors and DNA damage response (DDR) variants continue to be discovered. This presents an opportunity to apply hypothesis-free and unbiased methods to uncover new biological aspects of genome maintenance in human cells.

Recently, CRISPR-based methods and screens have emerged as powerful tools for investigating DDR mechanisms.

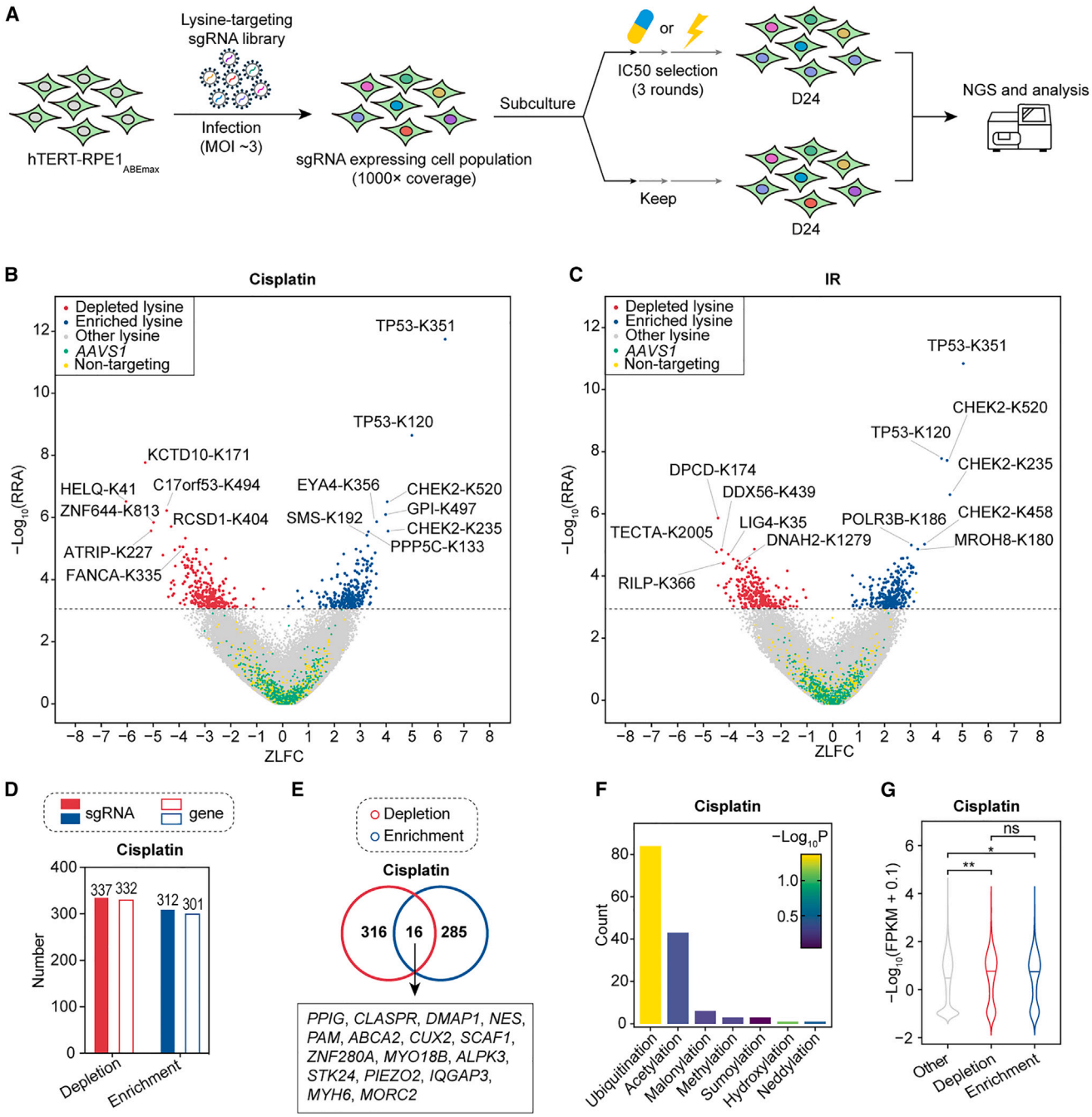

Figure 1. Comprehensive screening for genome-wide functional lysine residues and validation of the DDR

(A) Schematic overview of the screens conducted in RPE1 cells.

(B and C) Volcano plots depicting the overall results of functional lysine residues from the Lysine_Cisplatin (B) and Lysine_IR (C) screens. sgRNAs with significant negative selection (zLFC < 0) are marked in red, while those with significant positive selection (zLFC > 0) are marked in blue, under the threshold of RRA < 0.001. Green dots indicate sgRNAs targeting *AAVS1*, and yellow dots represent non-targeting sgRNAs. Specific top-ranked sgRNAs in both directions are individually labeled.

(D) The number of depleted (red) and enriched (blue) sgRNAs, along with their associated genes, identified in the Lysine_Cisplatin screen.

(E) Venn diagram illustrating the lysine residues selected within the gene context in the Lysine_Cisplatin screen, highlighting genes with lysine residues selected in different directions.

(F) Bar graphs displaying the number of PTMs at selected lysine residues, based on the PhosphoSite database. The *p* values are determined using Fisher's exact test and adjusted with the Benjamini-Hochberg method.

(legend continued on next page)

Olivieri et al. conducted 31 CRISPR-Cas9 screens against 27 genotoxic agents in the retinal pigment epithelium 1 (RPE1) cell line, identifying 890 genes linked to sensitivity or resistance to DNA-damaging agents.[24] Cuella-Martin et al. employed CRISPR-dependent cytosine base editing screens, identifying over 2,000 single guide RNAs (sgRNAs) that generate nucleotide variants in 86 DDR genes, resulting in altered cellular fitness upon DNA damage.[25] While these studies provide a holistic view of the genetic landscape involved in DDR, the former study used an engineered RPE1 cell line with inactivated p53, limiting the exploration of p53's role in response to genotoxic stress. In the latter study, the focus was limited to specific genes or SNVs.

In this study, we combined CRISPR-mediated base editing with pooled screening technologies to comprehensively analyze human lysine residue mutations and protein-coding genes in response to DNA-damaging agents in a model human cell line. This resource will significantly enhance our understanding of DDR mechanisms and their implications in human pathology.

RESULTS

Genome-wide screen of functional lysine residues in DDR

Building on our recent efforts to identify functional lysine residues that influence cellular fitness on a genome-wide scale in the hTERT-RPE1 cell line,[26] we utilized the same sgRNA library to identify lysine residues whose mutations impact DNA damage repair (STAR Methods). A schematic representation of the screens is depicted in Figure 1A. Briefly, cells infected with the lentiviral sgRNA library at a multiplicity of infection (MOI) of 3 were divided into control and treated groups.[27] The control group remained untreated, while the treated groups were exposed to either a sublethal dose of cisplatin or IR. We conducted these screenings in RPE1 cells using both negative selection assays (viability) and positive selection assays (genotoxin resistance). For example, in the lysine cisplatin screen (referred to as Lysine_Cisplatin), cells were exposed to cisplatin every 6 days for 48 h, while in the screen investigating the response to IR (referred to as Lysine_IR), cells were irradiated every 6 days at a half-maximal inhibitory concentration (IC50) dose (Figures S1A and S1B).

Genomic DNA was extracted after 24 days of screening and subjected to next-generation sequencing (NGS) analysis to evaluate the screening outcomes. The NGS data were analyzed using the Z score of $\log_2$ (fold-change) of each sgRNA^{iBAR} (ZFC^{iBAR}) algorithm.[28] zLFC (Z score of log fold change) and RRA (robust rank aggregation) were calculated for each sgRNA. The RRAL (negative $\log_{10}$ of RRA) for each sgRNA was used to rank the sgRNAs based on their impact on the response to genotoxin (Table S1). Negative scores indicated lysine residues whose mutation led to depletion from the cell population after genotoxin exposure, while positive scores represented lysine residues whose mutation conferred a selective growth advantage in the presence of cisplatin or IR.

Following the screenings, we identified hits, categorizing sgRNAs with RRA < 0.001 as selected sgRNAs. Under this threshold, we identified 647 and 660 functional lysine residues in the DDR in the Lysine_Cisplatin and Lysine_IR screens, respectively (Figures 1B and 1C; Table S1). In the Lysine_Cisplatin screen, 337 lysine residues whose mutation induced sensitization and 310 lysine residues whose mutation resulted in resistance were identified (Figure 1D; Table S1). The corresponding numbers in the Lysine_IR screen were 327 and 333 (Figure S1C; Table S1). In the genomic context, within 16 genes, both depleted and enriched selected lysine residues were discovered (*PPIG*, *CLASPR*, *DMAP1*, *NES*, *PAM*, *ABCA2*, *CUX2*, *SCAF1*, *ZNF280A*, *MYO18B*, *ALPK3*, *STK24*, *PIEZO2*, *IQGAP3*, *MYH6*, and *MORC2*) (Figure 1E). Similarly, in the Lysine_IR screen, 20 genes contained lysine residues in both directions (*ZNF292*, *SRP72*, *AXIN2*, *TNRC18*, *TTN*, *GOLGA2*, *ABCF1*, *RNF40*, *SARS*, *TNS3*, *SUPT5H*, *OBSCN*, *COL5A3*, *PTPRF*, *FNDC1*, *TCOF1*, *NEB*, *EVPL*, *DYNC1H1*, and *PWP2*) (Figure S1D).

Subsequent analysis of potential PTMs on selected lysine residues using the Database of Protein Post-Translational Modifications (dbPTM)[29,30] revealed significant enrichment of ubiquitination in the cisplatin library (Figure 1F). Although the IR library contained several PTMs, no significant enrichment was observed (Figure S1E). Notably, genes targeted by either positively or negatively selected sgRNAs exhibited higher expression levels than others, suggesting that genes with elevated expression are more functionally implicated in DDR regulation (Figures 1G and S1F).

To validate the identified functional lysine sites in response to genotoxin, we conducted cell proliferation assays in RPE1 cells using individual sgRNAs selected from the top-ranked sgRNAs in both libraries under untreated and treated conditions (Figure 2A; Table S2). An sgRNA targeting the nonfunctional *AAVS1* locus served as the negative control. In the Lysine_Cisplatin screen, all top-ranked enriched sgRNAs conferred resistance to cisplatin, and the majority of top-ranked depleted sgRNAs induced sensitization to cisplatin. The validated rate was high, indicating the reliability of this screening process. However, a substantial decrease in validation rates was observed in the Lysine_IR screen (Figure S2), likely due to increased noise from IR exposure. To ensure scientific rigor, our subsequent analyses primarily focus on data from the cisplatin screening and the successfully validated sites from the Lysine_IR screen.

Gene-level analysis of the screens

To gain deeper insights into our data, we aggregated our perturbations from the lysine residue level to the gene level and conducted pathway analyses. Using Gene Ontology for functional term enrichment analyses, we found that lysine residues

(G) Violin plots exhibiting the distributions of gene expression in RPE1-ABEmax cells. Genes with depleted or enriched sgRNAs are highlighted in red or blue, respectively, while all other genes are represented in gray. The center line represents the median, and the shaded area indicates the kernel density estimate. The p value was calculated using the Wilcoxon test. Significance levels are indicated as $^*p < 0.05$, $^{**}p < 0.01$, $^{***}p < 0.001$, while "NS" denotes non-significant results. See also Figure S1.

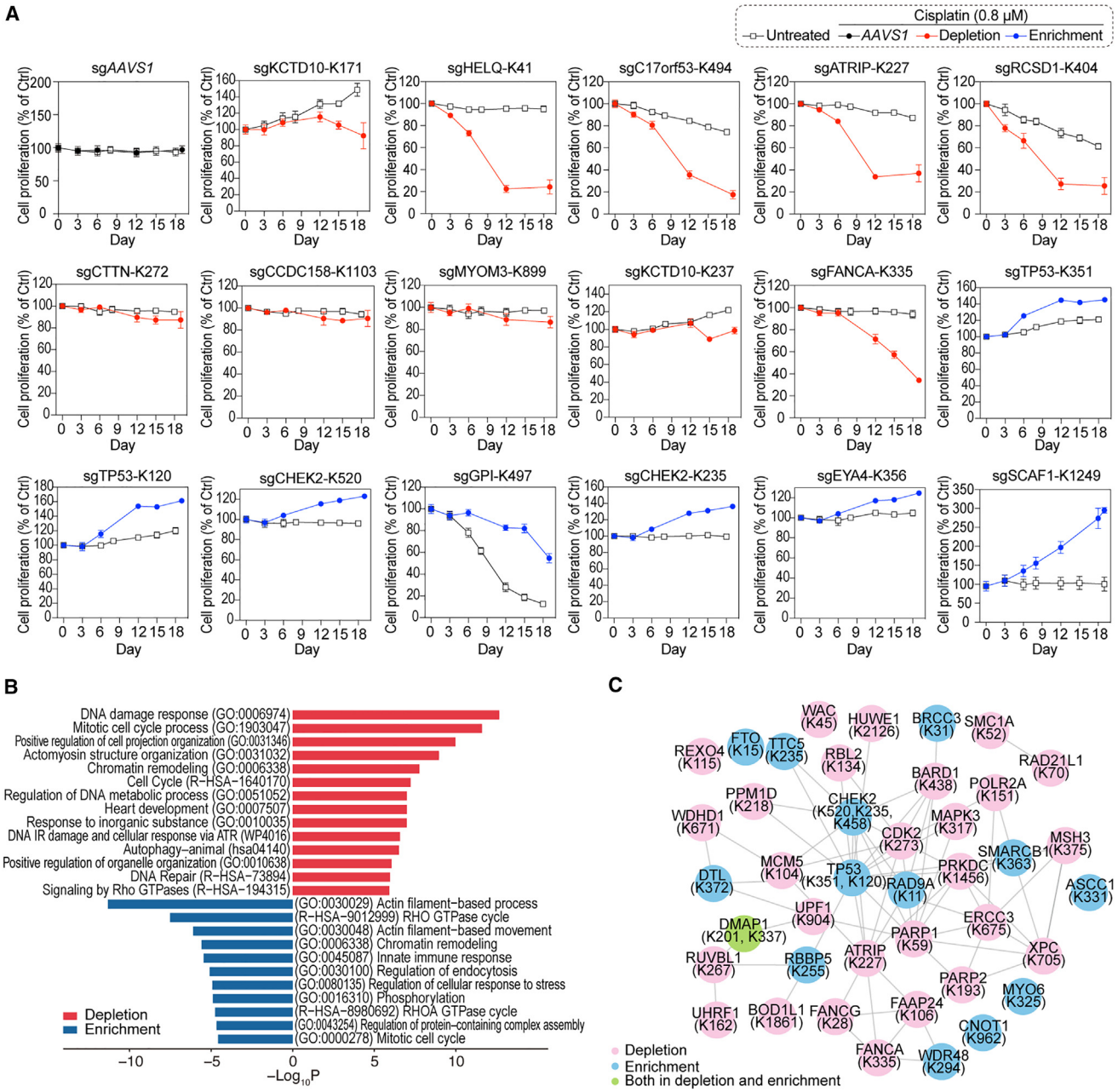

Figure 2. An overview of the DDR

(A) Validation of the top-ranked depleted (red) and enriched (blue) sgRNAs from the Lysine_Cisplatin screen using individual cell proliferation assays. Data are presented as mean ± SD; $n = 3$.

(B) Gene Ontology (GO) analysis of genes exhibiting depleted and enriched lysine mutations identified in the Lysine_Cisplatin screen.

(C) PPI network of genes featuring selected lysine mutations from the Lysine_Cisplatin screen. A specific subgroup of genes enriched in the GO analysis related to the cellular response to DNA damage stimulus is highlighted, with gene symbols and selected lysine residues indicated.

See also Figure S2.

depleted within gene contexts were significantly enriched in terms associated with mitotic processes across all evaluated categories (Figure 2B). Conversely, lysine residues enriched within gene contexts exhibited significant enrichment in processes related to actin filaments (Figure 2B). The diverse array of terms related to actin filaments suggests that previously unreported lysine mutations in actin may be linked to cisplatin resistance.

To further explore the role of these lysine residues in the response to cisplatin, we curated these selected lysine residues

CellPress
OPEN ACCESS

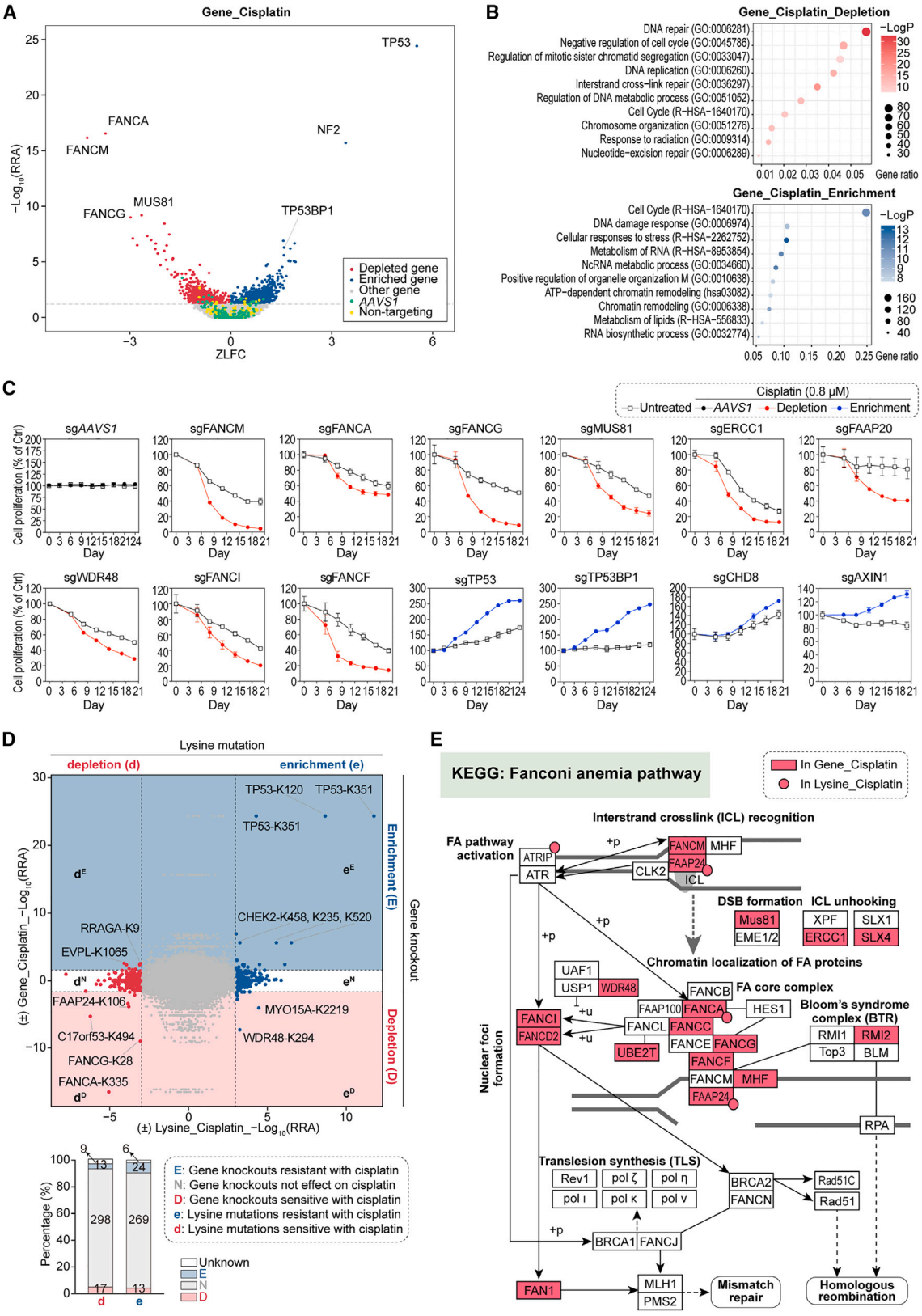

(legend on next page)

and performed a comprehensive bioinformatics analysis. Using Known and Predicted Protein-Protein Interactions (STRING) for protein-protein interaction (PPI) analysis, we found that proteins harboring these mutations formed a network associated with the cellular response to DNA damage stimuli (Figure 2C). This finding indicates a potential functional relationship between these mutated proteins and the cell's ability to detect and respond to DNA damage, possibly implicating them in key DNA repair or damage signaling pathways. Notably, the majority of these lysine mutations had not been identified previously. Therefore, our data not only provide a valuable resource for exploring cellular DNA repair regulation but also present a collection of potentially impactful lysine mutations for drug targeting.

BARBEKO-based gene knockout screen in response to genotoxins

In our targeted screens focusing on lysine residues, we identified numerous novel sites where the functional role of genes remains unexplored in the context of DNA damage repair. This prompted us to investigate whether these genes play specific roles in DNA repair. To address this, we conducted a gene knockout screen in the same cellular context. To reduce potential side effects associated with DNA double-strand breaks,[31–33] we employed the previously established iBARed cytosine base editing-mediated gene KO (BARBEKO) method.[28]

Using the ZFC^{iBAR} algorithm from the BARBEKO method,[28] we identified nearly 1,000 candidate genes whose knockout impacted the response to cisplatin (referred to as Gene_Cisplatin). As expected, we identified several well-known genes associated with DNA damage repair. For example, *TP53* was highlighted in positive selection, while genes involved in the Fanconi anemia (FA) pathway, such as *FANCA* and *FANCM*, were enriched in negative selection (Figure 3A; Table S3).

We then performed Gene Ontology analysis on the genes enriched in positive and negative selections. The analysis revealed that hits in negative selection were highly enriched in DNA repair-related terms, such as DNA repair (GO:0006281) and interstrand cross-link repair (GO:0036297), which aligns with the DNA interstrand cross-link damage induced primarily by cisplatin treatment[34] (Figure 3B). Meanwhile, the enriched genes in positive selection were largely related to cell cycle processes, which are known to influence the response to DNA damage (Figure 3B). Furthermore, we validated the top-ranking candidate genes using individual sgRNAs, all of which were successfully validated, demonstrating the high quality of the Gene_Cisplatin screen (Figure 3C; Table S2).

Annotation of functional lysine residues in the gene context

By comparing the results from both screens, we developed a head-to-head comparison diagram with specific thresholds based on their performance in response to DNA damage (Figure 3D; Table S3). To aid in identification, "E," "D," and "N" represent genes whose knockout led to resistance or sensitization or had no effect on the cellular response to genotoxins, respectively. "e" and "d" indicate resistance or sensitization of the cellular response to genotoxins following lysine residue mutations. Surprisingly, statistical analysis revealed that more than half of the identified lysine residues in the screening had no impact on cell proliferation after gene knockout, categorizing them as d^N or e^N.

Less than half of the mutants displayed phenotypes resembling the respective gene knockout effects, signifying a loss of function (LOF) due to the disruption of critical amino acids. However, some mutants showed the opposite effect by enhancing gene function. Notably, we identified 567 genes with no effect (N), with 298 lysine mutations leading to sensitization (d^N) and 269 lysine mutations leading to resistance (e^N), implying novel mechanisms of amino acid substitution that could be scarcely observed in traditional gene knockout screens (Figure 3D). We conducted cell proliferation assays to validate additional categories of lysine mutation vs. knockout (KO) comparisons, including d^E, e^D, d^N, and e^N. The results showed that, while some validation outcomes aligned with the screening results, others were suboptimal (Figure S3). We hypothesize that this discrepancy may be due to the lower ranking of certain sgRNAs.

Given that cisplatin primarily induces DNA interstrand cross-link damage, which activates the FA pathway for DNA damage repair, we observed that the Gene_Cisplatin and Lysine_Cisplatin screens identified numerous genes or lysine residues associated with this pathway, all in the negative direction. To illustrate this, we depicted the FA pathway and highlighted our selected genes and lysine residues using rectangles and circles, respectively (Figure 3E). Additionally, certain lysine residues were identified without corresponding gene-level effects, such as ATRIP-K227, and vice versa. This underscores the unique strengths and limitations of each screening method. Overall, our data provide a valuable resource for studying DDR

Figure 3. Annotation of selected lysine residues within the gene context

(A) Volcano plot illustrating the overall results from the Gene_Cisplatin screen. sgRNAs with significant negative selection (zLFC < 0) are marked in red, while those with significant positive selection (zLFC > 0) are marked in blue, under the threshold of RRA < 0.05. Green dots represent sgRNAs targeting *AAVS1*, and yellow dots indicate non-targeting sgRNAs. Several top-ranked sgRNAs in both directions are individually labeled.

(B) GO analysis of selected genes showing depletion (top) and enrichment (bottom) in the Gene_Cisplatin screen.

(C) Validation of the top-ranked depleted (red) and enriched (blue) sgRNAs from the Gene_Cisplatin screen using individual cell proliferation assays. Data are shown as mean ± SD; $n = 3$.

(D) Scatterplot illustrating the distribution of RRAL ($-\log_{10}$(RRA)) values for lysine residues (x axis) and their corresponding genes (y axis). Dashed lines mark the threshold for each screen, dividing the scatterplot into distinct areas. Six regions are labeled in the x^Y format: e or d indicate lysine mutations that enhance or decrease cellular sensitivity to cisplatin, respectively; E, D, or N indicate genes whose KO enhances, decreases, or has no effect on cellular sensitivity to cisplatin, respectively.

(E) Schematic of the Fanconi anemia (FA) signaling pathway. Red circles and rectangles denote selected lysine residues or genes in depletion, respectively. See also Figure S3.

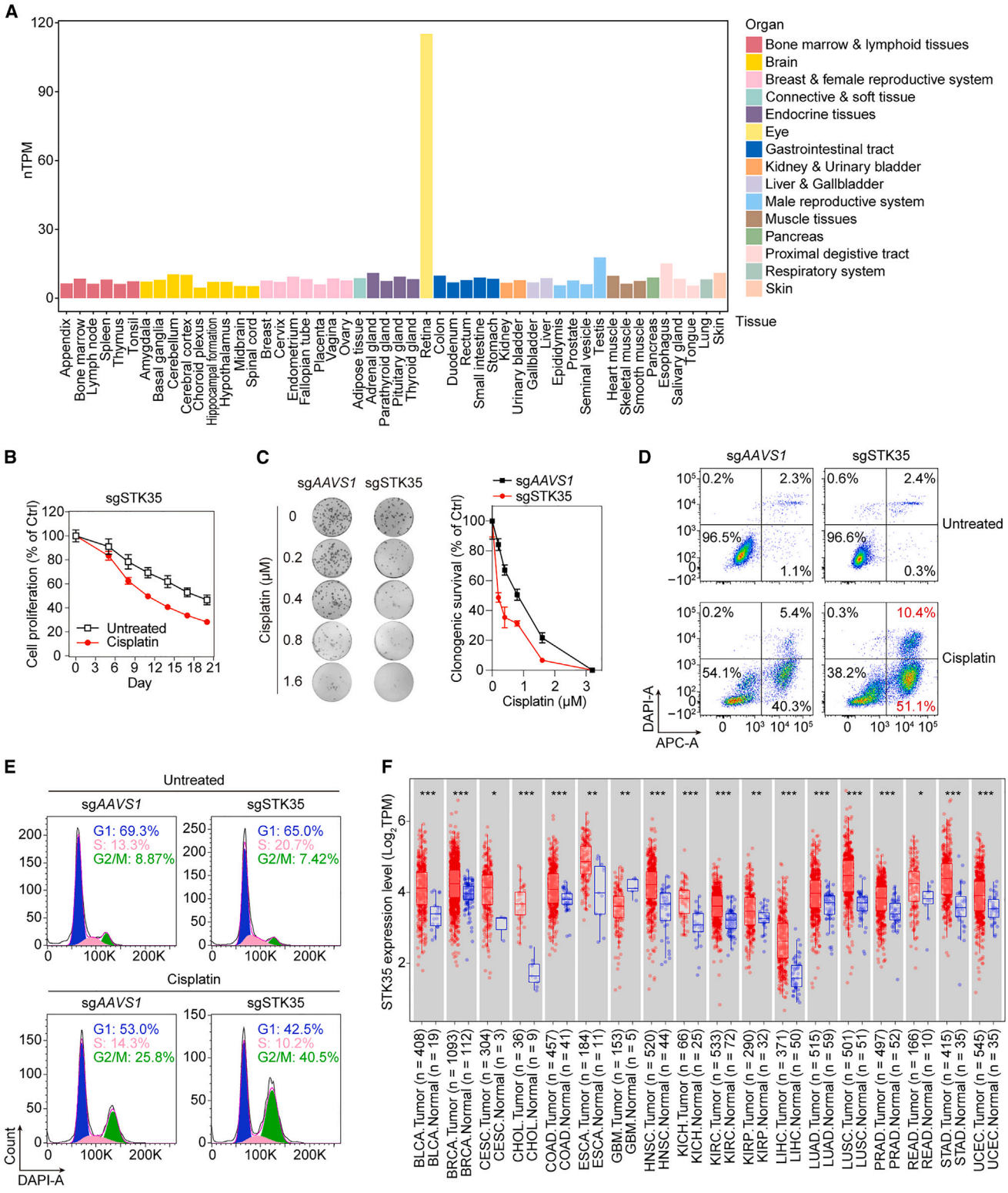

Figure 4. STK35 as potential modulator of the DDR

(A) Tissue-specific expression profile of STK35.

(B) Validation of cell proliferation effects in RPE1 cells using sgSTK35, both under untreated conditions and with cisplatin treatment (right, 0.8 μM). sg*AAVS1* serves as a negative control. Data are presented as mean ± SD; *n* = 3.

(legend continued on next page)

regulation and offer a repertoire of potentially critical lysine mutations for drug targeting.

STK35 as a candidate modulator of DDR

In our gene KO screen under cisplatin treatment, we identified *STK35* as a primary candidate (depletion rank 7), a gene previously unexplored in the context of DNA damage repair. Interestingly, we discovered that its tissue expression is particularly enriched in the retina, as indicated by the Human Protein Atlas (Figure 4A). Coincidentally, all of our screenings were conducted in RPE1 cell lines, which may explain why this gene has not been identified in prior screens. To investigate STK35's role in DNA repair, we conducted further experiments. Sanger sequencing analysis confirmed the effectiveness of three sgRNAs in generating *STK35* KO with AncBE4max (Figure S4A). Validation experiments subsequently affirmed that the absence of *STK35* increased sensitivity to cisplatin in RPE1 cells (Figures 4B and 4C). Remarkably, *STK35* KO also led to heightened cisplatin-induced apoptosis in RPE1-CRISPR cells compared to control cells (Figure 4D).

STK35 is a member of the new kinase family 4 Ser/Thr kinase (STK) family, classified within the "other" group in the human kinome.[35,36] Interestingly, literature suggests that STK19 and STK11, which belong to the same family as STK35, are associated with the transcription coupled NER (TC-NER) pathway[24,37] and UVB-induced damage sensing,[38,39] respectively. While the detailed biological functions of STK35 are still under investigation, existing studies suggest that it may act as a negative regulator of cell cycle progression,[40] potentially impeding the G1-to-S phase transition by modulating the expression of cell cycle proteins such as CDKN2A.[35,36] Consistently, in the absence of treatment, we observed a notable increase in the proportion of cells in the S phase following *STK35* KO (Figure 4E). Upon cisplatin treatment, *STK35*-deficient cells showed a marked increase in the G2/M phase compared to the control cells, suggesting that *STK35* deficiency leads to a greater tendency for cell-cycle arrest at G2/M in response to cisplatin-induced DNA damage.

We also conducted western blot analysis to assess DNA damage levels in *STK35* KO cells. Following cisplatin treatment, we observed decreased levels of γH2AX and S1981 phosphorylation of ATM (pATM-S1981) in *STK35* KO cells (Figures S4B and S4C). Additionally, no significant changes were detected in several other proteins related to DDR pathways (Figure S4D). Intriguingly, RNA levels of *STK35* were found to be higher in tumors compared to adjacent normal tissues across 18 cancer types (Figure 4F). Collectively, these data strongly suggest that STK35 likely plays a significant and complex role in DNA damage repair, highlighting the need for a comprehensive investigation of the specific molecular mechanisms involved.

Identification of known LOF variants in *TP53* and *CHEK2*

We investigated specific lysine residues in the e^E protein. The well-recognized "guardian" gene, *TP53*, is a prominent tumor suppressor that plays a key role in various pathways, including DNA damage repair and cell cycle regulation.[41–43] Our Lysine_Cisplatin and Lysine_IR screens identified two crucial sites: K351 and K120 (Figure 2A). K120 is a known acetylation site in p53, regulating its apoptotic function,[44] and the K120R mutation is known to inactivate p53.[45] Similarly, K351 is an acetylation site that significantly contributes to cell-cycle arrest.[46] We used NGS to explore the editing outcomes at these sites. The NGS results indicated high editing efficiency at both K351 and K120, with no bystander edits detected (Figure 5A). Consistent with previous reports,[26] mutations at TP53-K120 and K351 promoted cell proliferation under untreated conditions (Figure 2A). Notably, cells with mutations at these sites demonstrated increased resistance to cisplatin's cytotoxic effects (Figures 5B and 5C). These findings suggest that patients with tumors harboring mutations at TP53-K120 and K351 may face challenges with cisplatin-based therapies. Moreover, these p53 mutants (K351 and K120) did not affect protein stability (Figures 5D and 5E). The insights from this analysis provide valuable guidance for refining clinical treatment strategies, highlighting the complex relationship between specific lysine mutations, cell proliferation, and treatment resistance in cancer patients.

Our focus then shifted to the prominent *CHEK2* gene. The Lysine_Cisplatin and Lysine_IR screens identified K235, K458, and K520 as key lysine residues in CHK2 that contribute to a growth advantage in response to DNA damage. NGS results demonstrated high editing efficiency at all three sites (Figure 5F). These targeted lysine residues in CHK2 are highly conserved across species, including *Pan troglodytes* and *Macaca mulatta* (Figures S5A–S5C). Previous studies have linked *CHEK2* mutations to breast and ovarian cancer susceptibility and to Li-Fraumeni syndrome.[47–49] The CHK2 kinase, activated by ATM, plays a pivotal role in phosphorylating downstream substrates, particularly p53, to induce cell-cycle arrest in response to DNA damage.[11,50] In line with these findings, sgRNAs targeting *CHEK2* resulted in significant resistance to genotoxic agents (Figures 5G and 5H). During oxidative stress repair, acetylation at CHK2's K235 site triggers cell-cycle arrest until damage repair is completed.[51] Structural analysis reveals that K235 is located in the kinase domain of CHK2 (Figure 5I). Mutations at this site impair CHK2's kinase activity, preventing effective phosphorylation of downstream substrates such as CDC25, which, in turn, disrupts cell-cycle arrest and may promote cancer development (Figures 5J and S5D). This effect mirrors the outcomes observed with complete *CHEK2* KO,[52] leading to the accumulation of DNA mutations and potentially

(C) Clonogenic assay of BARBEKO_sgSTK35 in RPE1 cells upon cisplatin treatment (48 h). sg*AAVS1* serves as a negative control. Representative images are shown (left) with corresponding quantification (right). Data are presented as mean ± SD; $n = 3$.
(D) Apoptosis assessment of BARBEKO_sgSTK35 after cisplatin treatment (30 μM, 48 h).
(E) Cell cycle analysis of BARBEKO_sgSTK35 in RPE1 cells following cisplatin treatment (4 μM), with G1, S, and G2/M phases represented in blue, pink, and green, respectively.
(F) Differential expression analysis of human STK35 between tumor tissues (red) and adjacent normal tissues (blue) using TIMER2.0. The p value is calculated using the Wilcoxon test. Significance levels are indicated as $^*p < 0.05$, $^{**}p < 0.01$, $^{***}p < 0.001$. TPM, transcripts per million.
See also Figure S4.

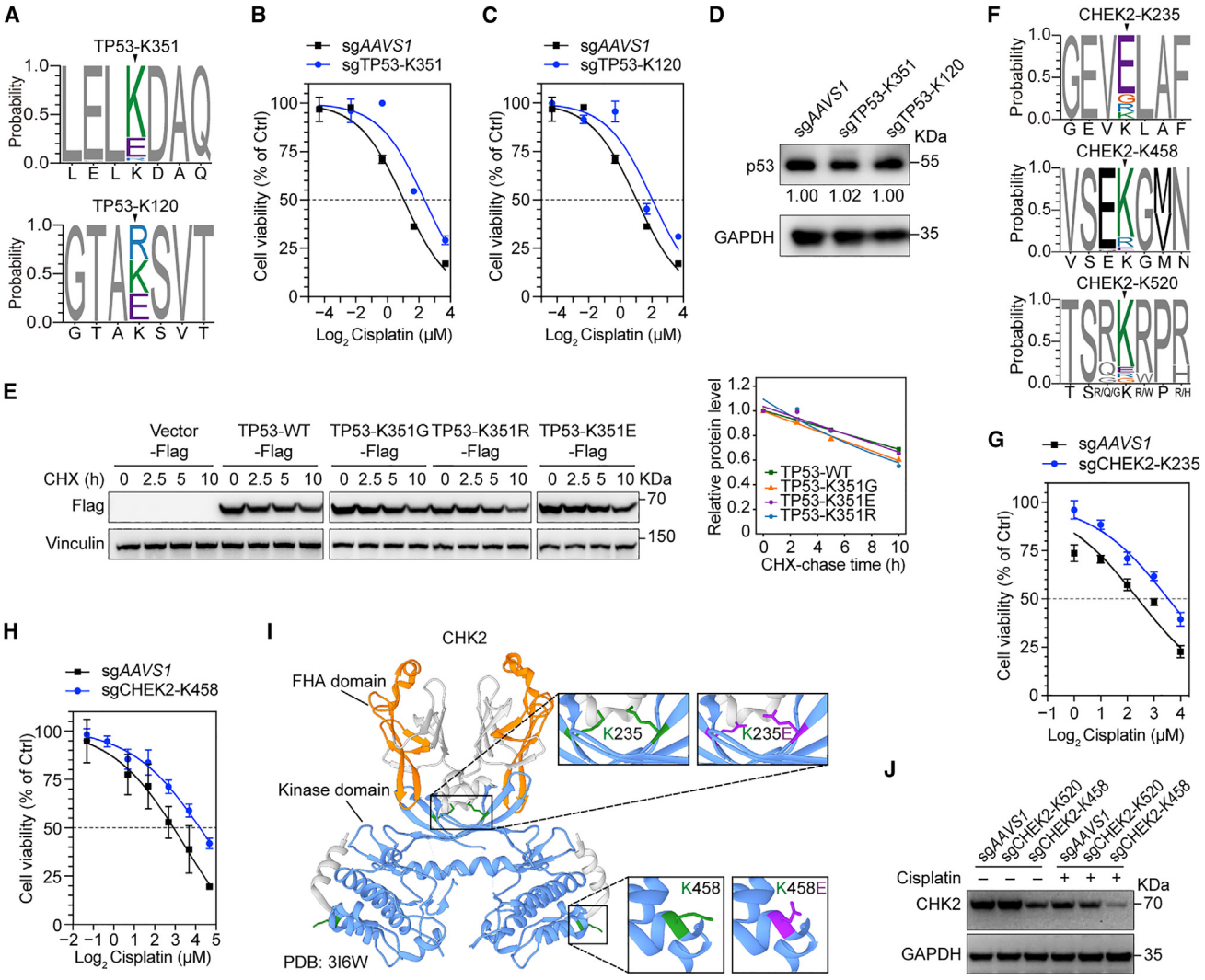

Figure 5. Characterization of *TP53* and *CHEK2*

(A) NGS analysis was performed on the editing outcomes of sgTP53-K351 and K120. The results are visualized as sequence logos, with amino acids denoted by single-letter codes. The reference sequences from cells expressing sg*AAVS1* are displayed below the x axis, with targeted lysine residues centered within the sequences. Gray shading indicates the three residues upstream or downstream of the targeted lysine sites when no editing is detected, while unintended editing outcomes are highlighted in black.

(B and C) The drug response of sgTP53-K120 and K351 in RPE1 cells was evaluated upon cisplatin treatment using CellTiter-Glo (CTG) cell viability detection. sg*AAVS1* serves as a control. Data are presented as mean ± SD; $n = 3$.

(D) Endogenous p53 protein abundance in RPE1 cells was detected through immunoblot analysis. Quantification was performed using ImageJ software and normalized to the glyceraldehyde-3-phosphate dehydrogenase (GAPDH) levels of each sample.

(E) The impact of K135R/E/G mutation on p53 protein stability was analyzed. Left: immunoblot analysis of TP53-WT, TP53-K351G, TP53-K351R, and TP53-K351E protein levels at various time points following cycloheximide (CHX) treatment. Right: relative protein levels of WT and mutant TP53 proteins at each time point after CHX treatment, normalized to the 0 h level. Quantification was performed using ImageJ software and normalized to vinculin levels of each sample.

(F) NGS analysis was conducted on the editing outcomes of sgCHEK2-K235, K458, and K520.

(G and H) The drug response of sgCHEK2-K235 and K458 in RPE1 cells was assessed following cisplatin treatment with CTG cell viability detection. sg*AAVS1* serves as a negative control. Data are shown as mean ± SD; $n = 3$.

(I) A crystal structure cartoon of the CHK2 dimer (PDB: 3I6W) with domains.

(J) Immunoblot analysis was used to assess CHK2 levels in RPE1 cells expressing sgCHEK2-K458.

See also Figure S5.

advancing cancer progression. Additionally, we found that CHK2 K458 mutants, like K235 mutants, reduce the protein level of CHK2 (Figures 5J and S7D); however, the underlying mechanism requires further investigation.

These findings validated the screen results and emphasized the importance of confirming sgRNA-induced mutational outcomes. The data provide valuable insights into the function of DDR genes and demonstrate the potential of our screening

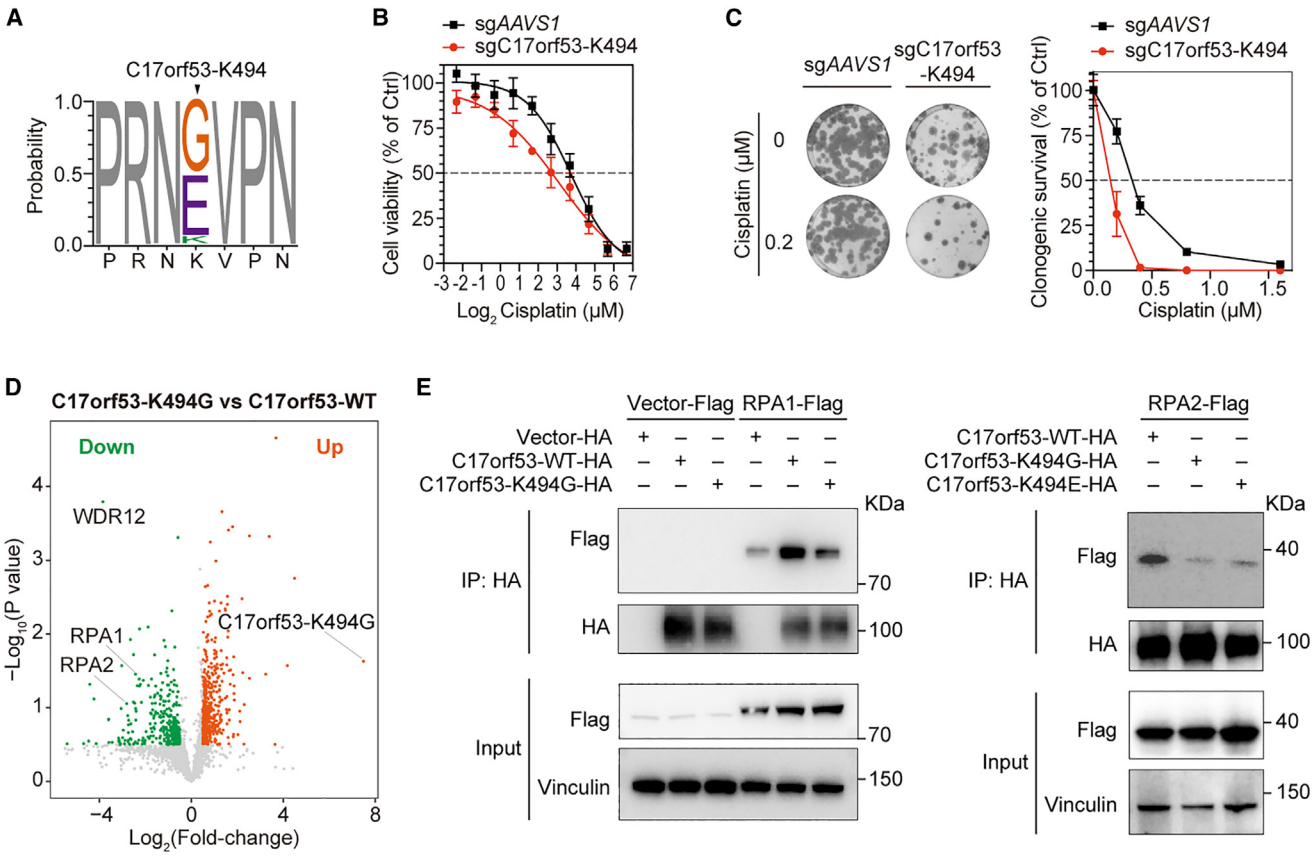

Figure 6. K494 of C17orf53 is crucial for DDR

(A) NGS analysis was conducted to assess the editing outcomes of C17orf53-K494 sgRNA.

(B) Cell proliferation was evaluated in RPE1 cells expressing sgC17orf53-K494, both without treatment (left) and following cisplatin treatment (right, 0.8 μM). sg*AAVS1* serves as a negative control. Data are presented as mean ± SD; $n = 3$.

(C) A clonogenic assay was conducted on RPE1 cells expressing sgC17orf53-K494 following cisplatin treatment (48 h). Representative images are displayed (left) with quantified results (right). Data are presented as mean ± SD; $n = 3$.

(D) Volcano plots depicting changes in interaction proteins in C17orf53-K494G compared to C17orf53-WT.

(E) Co-immunoprecipitation was performed to validate the interaction between C17orf53 and the RPA complex.

See also Figure S6.

approach in revealing the effects of clinically relevant mutations.

K494 of C17orf53 plays a vital role in DDR

Continuing our investigation, we delved into the lysine residues in d^D. Among our findings, K494, a lysine residue within the recently identified DNA repair gene *C17orf53*, stood out as previously undisclosed. Both the lysine residue and the gene itself ranked highly in the depletion direction of cisplatin screens. C17orf53, also known as HR with oligonucleotide/oligosaccharide-binding (OB) fold, has recently been recognized as a novel factor in DNA interstrand cross-link (ICL) repair.[53–55] It is recruited by RPA and single-stranded DNA (ssDNA) to function in the HR repair pathway in response to ICLs, subsequently recruiting the downstream MCM8-MCM9 helicase to facilitate DNA resection.

In our screen, C17orf53-K494 was identified as one of the most negatively selected lysine sites in response to cisplatin treatment. To validate the impact of the C17orf53-K494 mutation, we performed NGS of target sites and conducted cell proliferation assays using individual sgC17orf53-K494. The NGS results demonstrated high editing efficiency for sgC17orf53-K494, with no off-target edits observed (Figure 6A). We also observed that the C17orf53-K494 mutation slightly reduced protein expression levels (Figure S6A). Moreover, cell proliferation assays indicated that C17orf53-K494 mutant cells exhibited significantly reduced cell fitness upon cisplatin treatment (Figure 2A), consistent with the screening results. Further analysis of the drug-response curve using a Cell Counting Kit-8 assay in RPE1 cells confirmed that C17orf53-K494 mutant cells were indeed more sensitive to cisplatin treatment (Figure 6B), a finding that was further supported by a clonogenic survival assay (Figure 6C).

Given that C17orf53 has been identified as an S/G2-M-specific gene related to the cell cycle,[54] our cell cycle analysis revealed that C17orf53-K494 mutant cells experienced significant G2/M arrest upon cisplatin treatment (Figure S6B), suggesting

defective ICL repair in these cells. Additionally, K494 is located in the DNA binding domain OB fold of C17orf53, and the K494 mutation likely disrupts its recruitment by ssDNA. To further explore the impact of the C17orf53-K494 mutation, we conducted an affinity purification-mass spectrometry (AP-MS) assay using HEK293T cells transfected with C17orf53-wild type (WT) and C17orf53-K494G expression plasmids (Figure S6C). The comparison of interactomes revealed that C17orf53-K494G significantly impedes the interaction between C17orf53 and RPA1/2 (Figure 6D; Table S4), a finding further validated by a co-immunoprecipitation assay (Figure 6E).

Collectively, these data indicate that K494 is a newly identified crucial residue of C17orf53 and that its mutation disrupts the interaction of C17orf53 with its upstream factor RPA, resulting in profound ICL repair defect, G2/M cell-cycle arrest, and hypersensitivity to cisplatin treatment.

Representation of lysine mutations in cancer cases from the ICGC data portal

To explore the relationship between lysine residues and clinical mutations, we analyzed data from the International Cancer Genome Consortium (ICGC) database. Our analysis identified 106 selected lysine residues associated with 35 cancer types in the Lysine_Cisplatin screen (Figure 7A; Table S5) and 110 lysine residues linked to 34 cancer types in the Lysine_IR screen (Figure 7B; Table S5). Significantly, there are overlapping sites marked in red in both libraries, including well-studied residues such as TP53-K120 and TP53-K351. This finding highlights the significant role of these mutations in cancer patients and offers a valuable roadmap for developing informed clinical treatment strategies. However, it is noteworthy that there are inconsistencies in the sites related to ICGC between these two libraries, reflecting the distinct mechanisms of cisplatin and IR. Overall, these clinically relevant sites hold particular promise, especially in the context of tumor therapy.

We also conducted the Lysine_Cisplatin screen in another cell line, A375 (Figure S7A; Table S6). This screen identified 353 lysine residues in the depletion direction and 310 in the enrichment direction (Figures S7B and S7C). It is well recognized that cancer cells exhibit distinct differences in growth regulation compared to normal cells, with specialized pathways that control cell proliferation and survival, particularly under stress conditions like cisplatin treatment. Specifically, the A375 cell line harbors mutations in key genes, such as *BRAF*, which not only regulate cell proliferation but also influence the DDR, leading to differential activation of pathways following cisplatin-induced damage.

Gene Ontology (GO) analysis of our A375 screen results showed significant enrichment in pathways related to cell growth regulation (Figure S7D). A previous study that conducted a CRISPR-based gene KO screen in A375 cells to identify genes involved in the cisplatin-induced damage response[56] found results consistent with ours. They observed that few genes directly involved in DNA repair pathways were selected; instead, many were associated with the regulation of cell growth, underscoring the critical role of growth control pathways in mediating the cellular response to cisplatin. The study also noted differences in response pathways between cancerous and normal cell lines. As a result, our screens of A375 and RPE1 cells revealed few overlapping genes, reflecting the significant heterogeneity between normal and cancer cell lines (Figure S7E).

DISCUSSION

In this study, we utilized CRISPR-mediated base editing and pooled screening technologies to perform extensive analyses of human lysine residue mutations and protein-coding genes in response to DNA-damaging agents in a model human cell line. Unlike conventional CRISPR KO screens that focus on the gene as the unit of analysis, our approach permits the precise identification of functional protein residues, offering direct insights for mechanistic studies. Moreover, through the gene KO screen, we not only uncovered previously uncharacterized DNA repair factors but also identified well-established genes. Consequently, this resource greatly enhances our understanding of DDR mechanisms and their implications in human pathology.

Maintaining genome stability is a fundamental cellular requirement, and within our gene KO library, the discovery of the previously unreported gene *STK35*, which is highly conserved, is particularly noteworthy. KO out *STK35* increased cell sensitivity to cisplatin, resulting in an accumulation of cells in the G2/M phase, potentially due to impaired repair processes. The elevated expression of STK35 in colorectal cancer suggests its potential as a tumor biomarker, and further research is needed to understand its specific mechanisms, especially in combination with fluorouracil (5-FU) drug treatment, for potentially extending patient survival.

Regarding DNA repair factors, we identified several well-established genes, including *TP53* and *CHEK2*. PTMs add a critical layer of complexity to the proteome and play a critical role in DNA damage repair. Our screening strategy targeted lysine residues to identify sites associated with PTMs. Notably, we identified K235 of CHK2 as a potential acetylation site under oxidative stress. Additionally, our study confirmed K120 of p53 as an acetylation site that regulates p53's apoptotic function.

Moreover, this study corroborates several previous observations related to the FA repair pathway's response to cisplatin-induced ICLs. We identified multiple factors associated with the FA pathway that are crucial for ICL recognition and HR, such as FANCI, FANCD2, FANCM, FAAP24, FANCA, and FANCG. In addition to genes, we also identified novel lysine residue mutations in these factors that could potentially lead to increased sensitization to DNA-damaging agents. This study reinforces insights related to HR, particularly in the case of C17orf53, suggesting its role downstream of the RAD51 recombinase during HR in response to ICLs. The K494 mutation in C17orf53 was found to disrupt its interaction with the RPA protein, suggesting that this mutation might enhance the cisplatin sensitivity of tumor cells, making patients with this mutation more responsive to cisplatin chemotherapy.

Limitations of the study

It is important to acknowledge that our study offers only a partial perspective on the architecture of the human DDR, given the

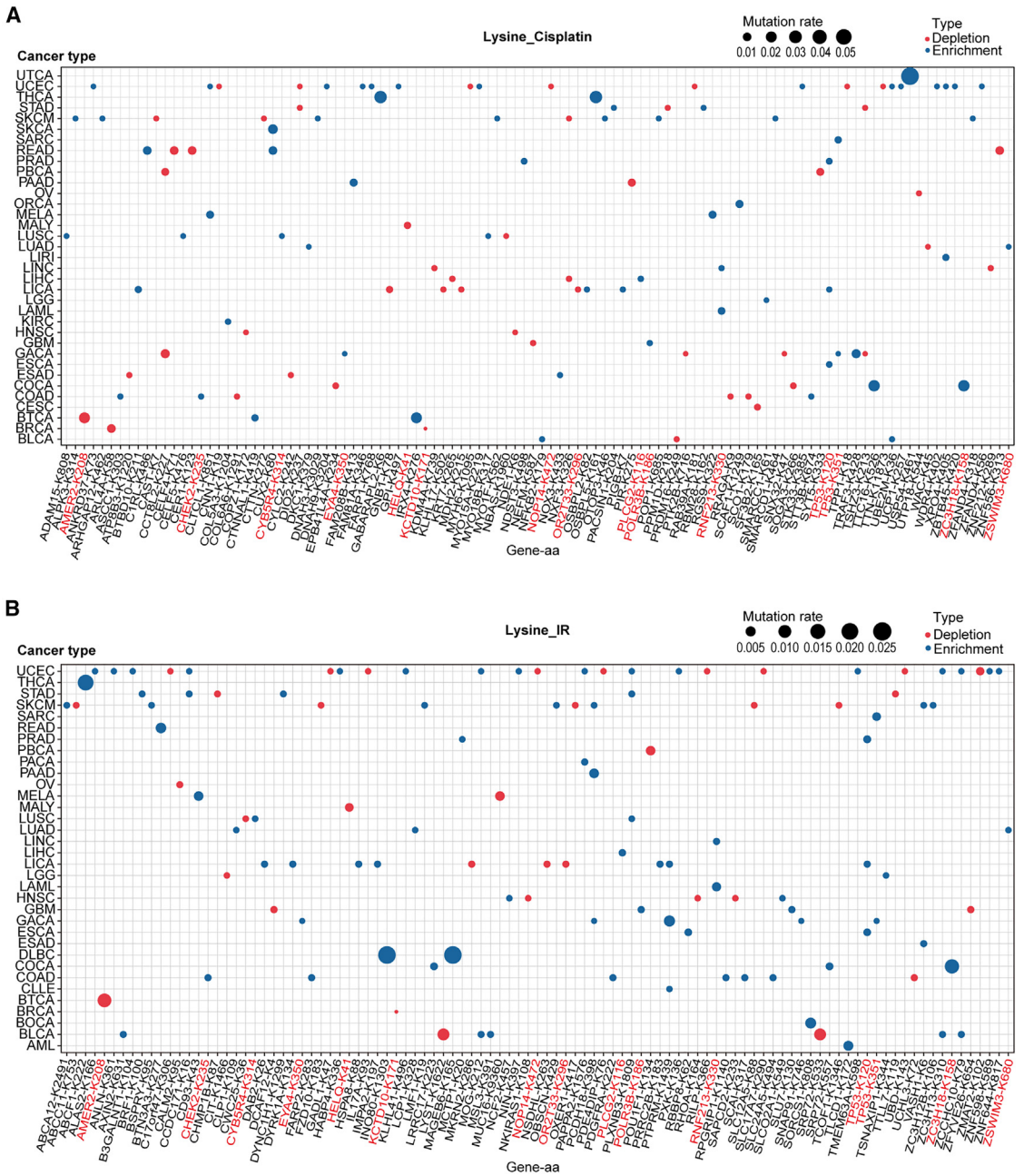

Figure 7. Clinical relevance of identified lysine sites

Diagram illustrating all identified sites with mutations detected in the ICGC database for the Lysine_Cisplatin screen (A) and Lysine_IR screen (B). The y axis lists various cancer types as defined by the ICGC, while the x axis features red labels indicating amino acids with common mutations in two screens. The size of each dot corresponds to the missense mutation rate detected for each amino acid.

See also Figure S7.

inherent technical constraints of our screening methods. A significant limitation is the reliance on just two cell lines, RPE1-hTERT and A375. Moreover, our study's scope is limited by the simplicity of employing only two genotoxic agents in the screens. Future research should expand to incorporate a wider range of agents and cell lines to provide more comprehensive and clinically relevant insights.

ABEmax has the ability to convert lysine into arginine, glutamic acid, or glycine. Arginine, like lysine, carries a positive charge and is often found at protein-DNA interaction sites due to its ability to form hydrogen bonds with DNA's phosphate groups. Glutamic acid, on the other hand, introduces a negative charge at physiological pH, while glycine is unique for lacking a chiral carbon, making it optically inactive and the smallest amino acid with

no side chain, resulting in neutrality and high flexibility. We observed bystander edits near the targeted lysine codons due to the susceptibility of all editable adenines within the "activity window," a common limitation in base editors-based screens that can potentially misattribute targeted lysine residues and lead to false positives.

In our initial validation using cell proliferation assays, several comparisons between gene KO and lysine mutation either failed to validate or showed only modest effects. We hypothesize that this discrepancy may be due to the lower ranking of certain sgRNAs. Additionally, the inherent randomness of DNA cleavage caused by IR introduces unpredictability and variability, which significantly affect the reproducibility of our verification results.

Another limitation is that we focused solely on lysine residues, which represent only one of the 20 amino acids. Notably, our group previously conducted a genome-wide screen to globally assess the cell fitness dependency on serine, threonine, and tyrosine residues.[57] In the future, we can investigate the functional roles of serine, threonine, tyrosine, and other amino acids in the DDR.

In summary, our study underscores the potential applications of the lysine residue library and the gene KO library. We successfully identified multiple lysine residues and genes that exhibit sensitivity or resistance to DNA-damaging agents. This comparative analysis offers valuable insights into the underlying mechanisms governing DNA damage repair processes.

RESOURCE AVAILABILITY

Lead contact

For additional information, resource requests, or reagents, please contact the lead contact, Wensheng Wei (wswei@pku.edu.cn), who will address and fulfill these requests.

Materials availability

All unique materials generated in this study can be obtained from the lead contact upon completion of a materials transfer agreement.

Data and code availability

- NGS data are available in the NCBI BioProject: PRJNA1180293. Data reported in this paper will be shared by the lead contact upon request.
- This paper does not report original code.
- Any further information required to reanalyze the data reported in this paper is available upon request from the lead contact.

ACKNOWLEDGMENTS

This research was financially supported by the National Science Foundation of China (NSFC31930016), the Peking-Tsinghua Center for Life Sciences, and Changping Laboratory (to W.W.). We are grateful to Y. Sun and C. Zhang (PKU) for supplying cell lines, the BIOPIC High-throughput Sequencing Center for performing NGS analysis, and the National Center for Protein Sciences (PKU) for their assistance with flow cytometry and mass spectrometry, especially H. Yang, H. Lyu, and D. Liu. We also appreciate the technical support provided by PKU's High-performance Computing Platform.

AUTHOR CONTRIBUTIONS

Conceptualization, W.W. and Z. Zhou; methodology, Q.P., Z. Zhang, Y.B., P.X., and Z.L.; software, Z.L.; validation, Q.P., Z. Zhang, Y.B., and T.C.; formal analysis, Q.P., Z. Zhang, Y.X., and Z.L.; investigation, Q.P., Z. Zhang, Y.B., T.C., P.X., H.M., and Y.Y.; writing – original draft, Q.P. and Z. Zhang; writing – review & editing, Q.P., Z. Zhang, F.X., and W.W.; visualization, Q.P., Z. Zhang, and Y.X.; supervision, W.W.

DECLARATION OF INTERESTS

W.W. is a scientific advisor and founder of EdiGene and Therorna.

STAR★METHODS

Detailed methods are provided in the online version of this paper and include the following:

- KEY RESOURCES TABLE
- EXPERIMENTAL MODEL AND STUDY PARTICIPANT DETAILS
- METHOD DETAILS
  - Plasmid construction
  - Library production
  - High-throughput screens of IR/Cisplatin treatment in RPE1 cells
  - Library data analysis
  - Editing efficiency detection by NGS
  - Cell proliferation assay
  - Immunoblotting
  - Cell cycle analysis
  - Clonogenic survival assay
  - Cell Titer Glo (CTG)
  - Cell Counting Kit-8 (CCK-8)
  - Immunoprecipitation
  - AP-MS assay
  - Apoptosis detection
  - CHX chase assay
- QUANTIFICATION AND STATISTICAL ANALYSIS

SUPPLEMENTAL INFORMATION

Supplemental information can be found online at https://doi.org/10.1016/j.celrep.2024.115047.

Received: January 28, 2024
Revised: September 5, 2024
Accepted: November 19, 2024

REFERENCES

1. Gupta, D., and Heinen, C.D. (2019). The mismatch repair-dependent DNA damage response: Mechanisms and implications. DNA Repair *78*, 60–69. https://doi.org/10.1016/j.dnarep.2019.03.009.
2. Lindahl, T., and Barnes, D.E. (2000). Repair of Endogenous DNA Damage. Cold Spring Harbor Symp. Quant. Biol. *65*, 127–133. https://doi.org/10.1101/sqb.2000.65.127.
3. Hustedt, N., and Durocher, D. (2016). The control of DNA repair by the cell cycle. Nat. Cell Biol. *19*, 1–9. https://doi.org/10.1038/ncb3452.
4. Chatterjee, N., and Walker, G.C. (2017). Mechanisms of DNA damage, repair, and mutagenesis. Environ. Mol. Mutagen. *58*, 235–263. https://doi.org/10.1002/em.22087.
5. Ciccia, A., and Elledge, S.J. (2010). The DNA Damage Response: Making It Safe to Play with Knives. Mol. Cell *40*, 179–204. https://doi.org/10.1016/j.molcel.2010.09.019.
6. Sfeir, A., and Symington, L.S. (2015). Microhomology-Mediated End Joining: A Back-up Survival Mechanism or Dedicated Pathway? Trends Biochem. Sci. *40*, 701–714. https://doi.org/10.1016/j.tibs.2015.08.006.
7. Caldecott, K.W. (2008). Single-strand break repair and genetic disease. Nat. Rev. Genet. *9*, 619–631. https://doi.org/10.1038/nrg2380.

8. Keenan, E.K., Zachman, D.K., and Hirschey, M.D. (2021). Discovering the landscape of protein modifications. Mol. Cell *81*, 1868–1878. https://doi.org/10.1016/j.molcel.2021.03.015.

9. Lee, J.M., Hammarén, H.M., Savitski, M.M., and Baek, S.H. (2023). Control of protein stability by post-translational modifications. Nat. Commun. *14*, 201. https://doi.org/10.1038/s41467-023-35795-8.

10. Song, H., Shen, R., Liu, X., Yang, X., Xie, K., Guo, Z., and Wang, D. (2023). Histone post-translational modification and the DNA damage response. Genes Dis. *10*, 1429–1444. https://doi.org/10.1016/j.gendis.2022.04.002.

11. Falck, J., Mailand, N., Syljuåsen, R.G., Bartek, J., and Lukas, J. (2001). The ATM–Chk2–Cdc25A checkpoint pathway guards against radioresistant DNA synthesis. Nature *410*, 842–847. https://doi.org/10.1038/35071124.

12. Bai, M., Ti, D., Mei, Q., Liu, J., Yan, X., Chen, D., Li, X., Wu, Z., and Han, W. (2020). The Role of Posttranslational Modifications in DNA Repair. BioMed Res. Int. *2020*, 1–13. https://doi.org/10.1155/2020/7493902.

13. Chatterjee, S., Senapati, P., and Kundu, T.K. (2012). Post-translational modifications of lysine in DNA-damage repair. Essays Biochem. *52*, 93–111. https://doi.org/10.1042/bse0520093.

14. Hanahan, D., and Weinberg, R.A. (2000). The Hallmarks of Cancer. Cell *100*, 57–70. https://doi.org/10.1016/S0092-8674(00)81683-9.

15. Di Micco, R., Fumagalli, M., Cicalese, A., Piccinin, S., Gasparini, P., Luise, C., Schurra, C., Garre', M., Nuciforo, P.G., Bensimon, A., et al. (2006). Oncogene-induced senescence is a DNA damage response triggered by DNA hyper-replication. Nature *444*, 638–642. https://doi.org/10.1038/nature05327.

16. Bartek, J. (2011). DNA damage response, genetic instability and cancer: From mechanistic insights to personalized treatment. Mol. Oncol. *5*, 303–307. https://doi.org/10.1016/j.molonc.2011.07.006.

17. Basu, A., and Krishnamurthy, S. (2010). Cellular Responses to Cisplatin-Induced DNA Damage. J. Nucleic Acids *2010*, 201367. https://doi.org/10.4061/2010/201367.

18. Rocha, C.R.R., Silva, M.M., Quinet, A., Cabral-Neto, J.B., and Menck, C.F.M. (2018). DNA repair pathways and cisplatin resistance: an intimate relationship. Clinics *73*, e478s. https://doi.org/10.6061/clinics/2018/e478s.

19. Hu, Q., and Hill, R.P. (1996). Radiosensitivity, Apoptosis and Repair of DNA Double-Strand Breaks in Radiation-Sensitive Chinese Hamster Ovary Cell Mutants Treated at Different Dose Rates. Radiat. Res. *146*, 636–645. https://doi.org/10.2307/3579379.

20. Santivasi, W.L., and Xia, F. (2014). Ionizing Radiation-Induced DNA Damage, Response, and Repair. Antioxidants Redox Signal. *21*, 251–259. https://doi.org/10.1089/ars.2013.5668.

21. Rothkamm, K., and Löbrich, M. (2003). Evidence for a lack of DNA double-strand break repair in human cells exposed to very low x-ray doses. Proc. Natl. Acad. Sci. USA *100*, 5057–5062. https://doi.org/10.1073/pnas.0830918100.

22. Hassin, O., and Oren, M. (2023). Drugging p53 in cancer: one protein, many targets. Nat. Rev. Drug Discov. *22*, 127–144. https://doi.org/10.1038/s41573-022-00571-8.

23. Lima, Z.S., Ghadamzadeh, M., Arashloo, F.T., Amjad, G., Ebadi, M.R., and Younesi, L. (2019). Recent advances of therapeutic targets based on the molecular signature in breast cancer: genetic mutations and implications for current treatment paradigms. J. Hematol. Oncol. *12*, 38. https://doi.org/10.1186/s13045-019-0725-6.

24. Olivieri, M., Cho, T., Álvarez-Quilón, A., Li, K., Schellenberg, M.J., Zimmermann, M., Hustedt, N., Rossi, S.E., Adam, S., Melo, H., et al. (2020). A Genetic Map of the Response to DNA Damage in Human Cells. Cell *182*, 481–496.e21. https://doi.org/10.1016/j.cell.2020.05.040.

25. Cuella-Martin, R., Hayward, S.B., Fan, X., Chen, X., Huang, J.-W., Taglialatela, A., Leuzzi, G., Zhao, J., Rabadan, R., Lu, C., et al. (2021). Functional interrogation of DNA damage response variants with base editing screens. Cell *184*, 1081–1097.e19. https://doi.org/10.1016/j.cell.2021.01.041.

26. Bao, Y., Pan, Q., Xu, P., Liu, Z., Zhang, Z., Liu, Y., Xu, Y., Yu, Y., Zhou, Z., and Wei, W. (2023). Unbiased interrogation of functional lysine residues in human proteome. Mol. Cell *83*, 4614–4632.e6. https://doi.org/10.1016/j.molcel.2023.10.033.

27. Zhu, S., Cao, Z., Liu, Z., He, Y., Wang, Y., Yuan, P., Li, W., Tian, F., Bao, Y., and Wei, W. (2019). Guide RNAs with embedded barcodes boost CRISPR-pooled screens. Genome Biol. *20*, 20. https://doi.org/10.1186/s13059-019-1628-0.

28. Xu, P., Liu, Z., Liu, Y., Ma, H., Xu, Y., Bao, Y., Zhu, S., Cao, Z., Wu, Z., Zhou, Z., and Wei, W. (2021). Genome-wide interrogation of gene functions through base editor screens empowered by barcoded sgRNAs. Nat. Biotechnol. *39*, 1403–1413. https://doi.org/10.1038/s41587-021-00944-1.

29. Lee, T.-Y., Huang, H.D., Hung, J.H., Huang, H.Y., Yang, Y.S., and Wang, T.H. (2006). dbPTM: an information repository of protein post-translational modification. Nucleic Acids Res. *34*, D622–D627. https://doi.org/10.1093/nar/gkj083.

30. Li, Z., Li, S., Luo, M., Jhong, J.-H., Li, W., Yao, L., Pang, Y., Wang, Z., Wang, R., Ma, R., et al. (2022). dbPTM in 2022: an updated database for exploring regulatory networks and functional associations of protein post-translational modifications. Nucleic Acids Res. *50*, D471–D479. https://doi.org/10.1093/nar/gkab1017.

31. Haapaniemi, E., Botla, S., Persson, J., Schmierer, B., and Taipale, J. (2018). CRISPR–Cas9 genome editing induces a p53-mediated DNA damage response. Nat. Med. *24*, 927–930. https://doi.org/10.1038/s41591-018-0049-z.

32. Ihry, R.J., Worringer, K.A., Salick, M.R., Frias, E., Ho, D., Theriault, K., Kommineni, S., Chen, J., Sondey, M., Ye, C., et al. (2018). p53 inhibits CRISPR–Cas9 engineering in human pluripotent stem cells. Nat. Med. *24*, 939–946. https://doi.org/10.1038/s41591-018-0050-6.

33. Brown, K.R., Mair, B., Soste, M., and Moffat, J. (2019). CRISPR screens are feasible in *TP 53* wild-type cells. Mol. Syst. Biol. *15*, e8679. https://doi.org/10.15252/msb.20188679.

34. Enoiu, M., Jiricny, J., and Schärer, O.D. (2012). Repair of cisplatin-induced DNA interstrand crosslinks by a replication-independent pathway involving transcription-coupled repair and translesion synthesis. Nucleic Acids Res. *40*, 8953–8964. https://doi.org/10.1093/nar/gks670.

35. Goyal, P., Behring, A., Kumar, A., and Siess, W. (2009). Identifying and Characterizing a Novel Protein Kinase STK35L1 and Deciphering Its Orthologs and Close-Homologs in Vertebrates. PLoS One *4*, e6981. https://doi.org/10.1371/journal.pone.0006981.

36. Vallenius, T., and Mäkelä, T.P. (2002). Clik1: a novel kinase targeted to actin stress fibers by the CLP-36 PDZ-LIM protein. J. Cell Sci. *115*, 2067–2073. https://doi.org/10.1242/jcs.115.10.2067.

37. Boeing, S., Williamson, L., Encheva, V., Gori, I., Saunders, R.E., Instrell, R., Aygün, O., Rodriguez-Martinez, M., Weems, J.C., Kelly, G.P., et al. (2016). Multiomic Analysis of the UV-Induced DNA Damage Response. Cell Rep. *15*, 1597–1610. https://doi.org/10.1016/j.celrep.2016.04.047.

38. Sapkota, G.P., Deak, M., Kieloch, A., Morrice, N., Goodarzi, A.A., Smythe, C., Shiloh, Y., Lees-Miller, S.P., and Alessi, D.R. (2002). Ionizing radiation induces ataxia telangiectasia mutated kinase (ATM)-mediated phosphorylation of LKB1/STK11 at Thr-366. Biochem. J. *368*, 507–516. https://doi.org/10.1042/bj20021284.

39. Esteve-Puig, R., Gil, R., González-Sánchez, E., Bech-Serra, J.J., Grueso, J., Hernández-Losa, J., Moliné, T., Canals, F., Ferrer, B., Cortés, J., et al. (2014). A Mouse Model Uncovers LKB1 as an UVB-Induced DNA Damage Sensor Mediating CDKN1A (p21WAF1/CIP1) Degradation. PLoS Genet. *10*, e1004721. https://doi.org/10.1371/journal.pgen.1004721.

40. Goyal, P., Behring, A., Kumar, A., and Siess, W. (2011). STK35L1 Associates with Nuclear Actin and Regulates Cell Cycle and Migration of Endothelial Cells. PLoS One *6*, e16249. https://doi.org/10.1371/journal.pone.0016249.

41. Levine, A.J. (1997). p53, the Cellular Gatekeeper for Growth and Division. Cell *88*, 323–331. https://doi.org/10.1016/S0092-8674(00)81871-1.

42. Kerrich, R. (1992). Continents ring the changes. Nature *358*, 16–17. https://doi.org/10.1038/358016a0.

43. Mantovani, F., Collavin, L., and Del Sal, G. (2019). Mutant p53 as a guardian of the cancer cell. Cell Death Differ. *26*, 199–212. https://doi.org/10.1038/s41418-018-0246-9.

44. Tang, Y., Luo, J., Zhang, W., and Gu, W. (2006). Tip60-Dependent Acetylation of p53 Modulates the Decision between Cell-Cycle Arrest and Apoptosis. Mol. Cell *24*, 827–839. https://doi.org/10.1016/j.molcel.2006.11.021.

45. Tang, Y., Zhao, W., Chen, Y., Zhao, Y., and Gu, W. (2008). Acetylation Is Indispensable for p53 Activation. Cell *133*, 612–626. https://doi.org/10.1016/j.cell.2008.03.025.

46. Beckerman, R., Yoh, K., Mattia-Sansobrino, M., Zupnick, A., Laptenko, O., Karni-Schmidt, O., Ahn, J., Byeon, I.-J., Keezer, S., and Prives, C. (2016). Lysines in the tetramerization domain of p53 selectively modulate G1 arrest. Cell Cycle *15*, 1425–1438. https://doi.org/10.1080/15384101.2016.1170270.

47. Antoni, L., Sodha, N., Collins, I., and Garrett, M.D. (2007). CHK2 kinase: cancer susceptibility and cancer therapy – two sides of the same coin? Nat. Rev. Cancer *7*, 925–936. https://doi.org/10.1038/nrc2251.

48. Bell, D.W., Varley, J.M., Szydlo, T.E., Kang, D.H., Wahrer, D.C., Shannon, K.E., Lubratovich, M., Verselis, S.J., Isselbacher, K.J., Fraumeni, J.F., et al. (1999). Heterozygous Germ Line *hCHK2* Mutations in Li-Fraumeni Syndrome. Science *286*, 2528–2531. https://doi.org/10.1126/science.286.5449.2528.

49. Apostolou, P., and Papasotiriou, I. (2017). Current perspectives on CHEK2 mutations in breast cancer. Breast Cancer *9*, 331–335. https://doi.org/10.2147/BCTT.S111394.

50. Hirao, A., Kong, Y.-Y., Matsuoka, S., Wakeham, A., Ruland, J., Yoshida, H., Liu, D., Elledge, S.J., and Mak, T.W. (2000). DNA Damage-Induced Activation of p53 by the Checkpoint Kinase Chk2. Science *287*, 1824–1827. https://doi.org/10.1126/science.287.5459.1824.

51. Kwon, J., Lee, S., Kim, Y.-N., and Lee, I.H. (2019). Deacetylation of CHK2 by SIRT1 protects cells from oxidative stress-dependent DNA damage response. Exp. Mol. Med. *51*, 1–9. https://doi.org/10.1038/s12276-019-0232-4.

52. Takai, H., Naka, K., Okada, Y., Watanabe, M., Harada, N., Saito, S., Anderson, C.W., Appella, E., Nakanishi, M., Suzuki, H., et al. (2002). Chk2-deficient mice exhibit radioresistance and defective p53-mediated transcription. EMBO J. *21*, 5195–5205. https://doi.org/10.1093/emboj/cdf506.

53. Wang, C., Chen, Z., Su, D., Tang, M., Nie, L., Zhang, H., Feng, X., Wang, R., Shen, X., Srivastava, M., et al. (2020). C17orf53 is identified as a novel gene involved in inter-strand crosslink repair. DNA Repair *95*, 102946. https://doi.org/10.1016/j.dnarep.2020.102946.

54. Hustedt, N., Saito, Y., Zimmermann, M., Álvarez-Quilón, A., Setiaputra, D., Adam, S., McEwan, A., Yuan, J.Y., Olivieri, M., Zhao, Y., et al. (2019). Control of homologous recombination by the HROB–MCM8–MCM9 pathway. Genes Dev. *33*, 1397–1415. https://doi.org/10.1101/gad.329508.119.

55. Huang, J.-W., Acharya, A., Taglialatela, A., Nambiar, T.S., Cuella-Martin, R., Leuzzi, G., Hayward, S.B., Joseph, S.A., Brunette, G.J., Anand, R., et al. (2020). MCM8IP activates the MCM8-9 helicase to promote DNA synthesis and homologous recombination upon DNA damage. Nat. Commun. *11*, 2948. https://doi.org/10.1038/s41467-020-16718-3.

56. Ko, T., and Li, S. (2019). Genome-wide screening identifies novel genes and biological processes implicated in cisplatin resistance. Faseb. J. *33*, 7143–7154. https://doi.org/10.1096/fj.201801534RR.

57. Li, Y., Xu, T., Ma, H., Yue, D., Lamao, Q., Liu, Y., Zhou, Z., and Wei, W. (2024). Functional profiling of serine, threonine and tyrosine sites. Nat. Chem. Biol. https://doi.org/10.1038/s41589-024-01731-0.

58. Li, T., Fu, J., Zeng, Z., Cohen, D., Li, J., Chen, Q., Li, B., and Liu, X.S. (2020). TIMER2.0 for analysis of tumor-infiltrating immune cells. Nucleic Acids Res. *48*, W509–W514. https://doi.org/10.1093/nar/gkaa407.

59. Koblan, L.W., Doman, J.L., Wilson, C., Levy, J.M., Tay, T., Newby, G.A., Maianti, J.P., Raguram, A., and Liu, D.R. (2018). Improving cytidine and adenine base editors by expression optimization and ancestral reconstruction. Nat. Biotechnol. *36*, 843–846. https://doi.org/10.1038/nbt.4172.

STAR★METHODS

KEY RESOURCES TABLE

REAGENT or RESOURCE	SOURCE	IDENTIFIER
Antibodies		
Rabbit polyclonal anti-FLAG	Sigma-Aldrich	Cat# F7425; RRID: AB_439687
Mouse monoclonal anti-TP53	Cell Signaling	Cat# 2524; RRID: AB_331743
Rabbit monoclonal anti-Vinculin	Abcam	Cat# ab129002; RRID: AB_11144129
Mouse monoclonal anti-C17orf53	Thermo Fisher Scientific	Cat# MA5-17037; RRID: AB_2538509
Mouse monoclonal anti-CHEK2	Cell Signaling	Cat# 3440; RRID: AB_2229490
Rabbit monoclonal anti-GAPDH	EASYBIO	Cat# BE3407; RRID: AB_3075319
Rabbit polyclonal anti-HA	Sigma-Aldrich	Cat# H6908; RRID: AB_260070 Cat# SAB4300603; RRID: AB_10620829
Mouse monoclonal anti-phospho-Histone H2A.X (Ser139)	Millipore	Cat# 05–636; RRID: AB_309864
Rabbit monoclonal anti-ATM (phospho S1981)	Abcam	Cat# ab81292; RRID: AB_1640207
Rabbit monoclonal anti-ATM	Cell Signaling	Cat# 2873; RRID: AB_2062659
Mouse monoclonal anti-RAD51	Cell Signaling	Cat# 8875; RRID: AB_2721109
Rabbit monoclonal anti-CCNB1	Cell Signaling	Cat# 12231; RRID: AB_2783553
Rabbit monoclonal anti-PLK1	Cell Signaling	Cat# 4513; RRID: AB_2167409
Mouse monoclonal anti-p21	Cell Signaling	Cat# 2946; RRID: AB_2260325
Rabbit monoclonal anti-p16	Cell Signaling	Cat# 80772; RRID: AB_2799960
Bacterial and virus strains		
Trans1-T1 phage resistant chemically competent cell	TransGen Biotech	Cat# CD501
E. coli HST08 premium electro-cells	TaKaRa	Cat# 9028
Chemicals, peptides, and recombinant proteins		
Gibson Assembly® Master Mix	New England Biolabs	Cat# E2611
Cisplatin	Selleck	Cat# 15663-27-1
T4 DNA Ligase	New England Biolabs	Cat# M0202
X-tremeGENE HP DNA transfection reagent	Roche	Cat# 06366236001
Puromycin	Solaribio	Cat# P8230
Passive lysis buffer	Promega	Cat# E1941
Phosphatase inhibitor cocktail	Thermo Fisher Scientific	Cat# 78441
Cycloheximide	Sigma-Aldrich	Cat# 5087390001
CellTiter-GloO® 2.0	Promega	Cat# G9242
EZview™ Red Anti-HA Affinity Gel	Sigma-Aldrich	Cat# E6779
Reducing SDS loading buffer	CWBIO	Cat# CW0027
Non-reducing SDS loading buffer	CWBIO	Cat# CW0028
Critical commercial assays		
DNeasy Blood and Tissue Kit	Qiagen	Cat# 69506
KAPA HiFi HotStart ReadyMix PCR Kit	Roche	Cat# KK2602
DNA Clean & Concentrator-5	Zymo Research Corporation	Cat# D4013
NEBNext Ultra II Q5 Master Mix	New England Biolabs	Cat# M0544
Clarity Western ECL Substrate Kit	Bio-Rad	Cat# 1705060
Pierce BCA Protein Assay Kit	Thermo Fisher Scientific	Cat# 23225

(*Continued on next page*)

Continued

REAGENT or RESOURCE	SOURCE	IDENTIFIER
Deposited data		
NGS data	This study	NCBI BioProject accession: No. PRJNA1180293
Experimental models: Cell lines		
HEK293T	ATCC	N/A
hTERT-RPE1	Y. Sun's laboratory, Peking University	N/A
hTERT-RPE1-ABEmax-SC	This study	N/A
hTERT-RPE1-AncBE4max SC	This study	N/A
Recombinant DNA		
pCMV-ABEmax-P2A-GFP	Addgene	Cat# 112101
pLenti-ABEmax-EGFP	This study	N/A
pCG-2.0-CMV-mCherry	This study	N/A
pLenti-cDNA-Flag-mCherry	This study	N/A
pLenti-cDNA-HA-EGFP	This study	N/A
pVSV-G	Addgene	N/A
pR8.74	Addgene	N/A
pCG-2.0-SV40-Puro-iBAR-1	This study	N/A
pCG-2.0-SV40-Puro-iBAR-2	This study	N/A
pCG-2.0-SV40-Puro-iBAR-3	This study	N/A
Software and algorithms		
ImageJ	National Institutes of Health	https://imagej.nih.gov/ij/
FlowJo	BD Biosciences	https://www.bdbiosciences.com/en-us/products/software/flowjo-v10-software
STRING	Global Biodata Coalition and ELIXIR	https://string-db.org/
Cytoscape	Cytoscape	Cytoscape
Prism 9	Graphpad	https://www.graphpad.com/features
R (v3.4.1, v3.5.0)	R	https://www.r-project.org
Python (v2.7, v3.8)	Python	https://www.python.org
Chimera	Resource for Biocomputing, Visualization, and Informatics	https://www.cgl.ucsf.edu/chimera/
Adobe Illustrator	Adobe	https://www.adobe.com/products/illustrator.html
Adobe Photoshop	Adobe	https://www.adobe.com/products/photoshop.html
Image Lab	Bio-Rad	https://www.bio-rad.com/zh-cn/product/image-lab-software?ID=KRE6P5E8Z
Timer2.0	Li et al.[58]	http://timer.cistrome.org

EXPERIMENTAL MODEL AND STUDY PARTICIPANT DETAILS

The HEK293T cell line was obtained from ATCC, while the hTERT-RPE1 cell line was provided from Yujie Sun's laboratory. HEK293T cells were cultured in DMEM (Dulbecco's modified Eagle's medium, Gibco, Thermo Fisher Scientific) supplemented with 10% (v/v) bovine growth serum (Biological Industries) and 1% penicillin-streptomycin (Thermo Fisher Scientific). The hTERT-RPE1 cells were grown in DMEM/F12 (Gibco, Thermo Fisher Scientific) supplemented with 10% (v/v) bovine growth serum (Biological Industries) and 1% penicillin-streptomycin (Thermo Fisher Scientific). All cells were maintained in a humidified atmosphere at 37°C with 5% CO_2 and were confirmed to be mycoplasma-free.

METHOD DETAILS

Plasmid construction

To construct pCMV_ABEmax_P2A_EGFP for genome editing, ABEmax (from Addgene, #112101) was cloned into the pLenti_P2A_EGFP vector using double restriction enzymes digestion (New England Biolabs) and T4 ligase ligation (NEB, #M0202).

AncBE4max was sourced from Koblan et al.'s supplementary information[59] and synthesized by Synbio Technologies. AncBE4max sequence was cloned into pLenti_P2A_mCherry vector using the same cloning method. Individual sgRNA oligos were synthesized by Ruibotech and cloned into the pCG2.0-sgRNA-expressing vector via Golden Gate assembly. C17orf53 and STK35 coding sequences were cloned into pLenti-cDNA-flag-mCherry or pLenti_cDNA_HA_EGFP backbones using PCR and Gibson assembly (NEB, #E2611). Base substitutions for mutants were introduced via PCR mutagenesis.

Library production

The oligonucleotide pool was synthesized by Synbio Technologies. SgRNA sequences were PCR amplified with primers targeting the flanking sequences of the oligos.[26] These sgRNAs were cloned into three types of pLenti-sgRNA^{iBAR} vectors using Golden-Gate assembly. Three verified iBARs were used in this library: CTCGCT, GATGGT, and GCACTG (5′-3′). The Golden-Gate products were purified and electroporated into competent cells (TaKaRa, #9028) for library plasmid production, which were co-transfected with viral packaging plasmids pVSVG and pR8.74 (Addgene).

High-throughput screens of IR/Cisplatin treatment in RPE1 cells

For the lysine functional screen under IR/Cisplatin treatment, ABEmax-expressing RPE1 cells were infected with the lentiviral library at a high MOI (~3). 72 h post-infection, infected cells were selected with puromycin (15 μg/mL) for two days. Viable cells were harvested as the reference group (Day 0), and the remaining cells were split into fitness, IR treatment, and cisplatin treatment groups. The library cells were passaged every 3 days, until Day 24, and maintained at 1,000-fold coverage. In treatment groups, IC50 doses of IR (1.9 Gy) or cisplatin (0.8 μM) were administered every six days. Genomic DNA was extracted from the cell pellets using the Dneasy Blood and Tissue Kit (Qiagen, #69506). Genomic-integrated sgRNA sequences were amplified by PCR using KAPA HiFi HotStart ReadyMix PCR Kit (Roche, #KK2602). The used PCR condition was: 30 s at 95°C; followed by 10 s at 95°C, 30 s at 60°C, 15 s at 72°C for 26 cycles, and 15 s at 72°C. PCR products were purified by DNA Clean & Concentrator-5 (Zymo Research Corporation, D4013), followed by NGS analysis.

For genome-scale gene knockout screen upon cisplatin treatment, we used BARBEKO sgRNA library to perform screening in RPE1 cells.[28] Cells were plated onto 15-cm plates and infected by lentiviral sgRNA library at MOI of 3. The library cells were treated by puromycin (15 μg/mL) for 48 h selection. Then, a library size of cells was harvested as the reference group, denoted as Day 0. The rest of the library cells were also divided into fitness, IR treatment, and cisplatin treatment groups, and passaged every 3 days. IC50 dose of cisplatin (0.8 μM) was added every 6 days and the experimental cells were harvested on Day 15.

Library data analysis

We utilized the ZFC^{iBAR} algorithm, used in the BARBEKO screen, to analyze the data. This method uses the zLFC (*Z* score of Log_2 Fold Change) to evaluate changes in sgRNA^{iBAR} abundance between the reference and the experimental groups.

First, raw counts of sgRNA^{iBAR} were adjusted using either total-count normalization or median-ratio normalization to correct batch effects. sgRNAs^{iBAR} with counts <0.05th quantile in the distribution of both reference and experimental groups were defined as small count sgRNAs^{iBAR}. The mean count of these small count sgRNAs^{iBAR} was added to all sgRNAs^{iBAR} to mitigate the impact of small count on LFC in the reference group.

Second, the LFC of each sgRNA^{iBAR} was calculated as follows:

$$\text{sgRNA}^{iBAR}\text{LFC} = \log_2\frac{\text{normC}_{exp}+\text{normC}_{small}}{\text{normC}_{ref}+\text{normC}_{small}}$$

where normC_{exp} and normC_{ref} represent the normalized counts of sgRNAs^{iBAR} in the experimental and reference groups, respectively, and normC_{small} is the normalized mean count of small-count sgRNAs^{iBAR}.

Third, to calculate the standard deviation (s.d.) for *Z* score normalization, the sgRNA^{iBAR} LFC values were divided into bins based on their counts in the reference group. A linear model was then fitted to calculate the LFC s.d. for all sgRNAs^{iBAR}. Inspired by Colic et al., the zLFC was calculated as follows:

$$\text{sgRNA}^{iBAR}\ \text{zLFC} = \frac{\text{sgRNA}^{iBAR}\text{LFC}}{\text{LFC}_{std}}$$

where LFC_{std} is the s.d. derived from the linear model. The empirical *p* value for sgRNA^{iBAR} zLFC was then calculated.

Fourth, the zLFC for sgRNAs was calculated as the mean of the zLFC values for the corresponding sgRNAs^{iBAR}. Subsequently, the gene zLFC was determined as the mean zLFC of the corresponding sgRNAs. sgRNA zLFC $= \frac{\text{sgRNA}^{iBAR}\text{LFC}}{n}$

$$\text{Gene zLFC} = \frac{\text{sgRNA zLFC}}{m}$$

where n is the number of sgRNAs^{iBAR} associated with a certain sgRNA (equal to 4 in this study's BARBEKO strategy), and m is the number of sgRNAs associated with a certain gene (equal to 3 in this study).

Fifth, the RRA was utilized to rank the significance of a certain sgRNA or gene by ranking sgRNAs[iBAR] across the whole library. For bidirectional screens, RRA was calculated separately for enrichment and depletion.

Editing efficiency detection by NGS

The genomic regions flanking the targeted lysine codons were PCR amplified and sent for NGS. Editing efficiency of targeted residues was assessed by mapping FASTQ files to PCR target regions using BWA. All the mapped reads were piled up with in-house scripts. The nucleotides around the target codons were extracted from the pile-up files and translated into protein sequences. The seqlogo graphs of the protein sequences were generated using WebLogo 3.

Cell proliferation assay

sgRNAs were cloned into a lentivirus backbone with mCherry or EGFP markers and packaged into lentivirus in HEK293T cells. ABEmax- or AncBEmax-expressing RPE1 cells were infected by individual sgRNA lentivirus at 40–60% efficiency. Cell percentages were measured by flow cytometry every three days, with cisplatin (0.8 μM) or IR (1 Gy) treatment applied after passage. The first flow cytometry was performed at three days after transfection, denoted as Day 0. Data were represented as the percentage of $mCherry^+$ or $EGFP^+$ normalized to Day 0.

Immunoblotting

Cells were lysed with Passive Lysis Buffer (Promega, #E1941), and proteins were resolved via SDS-PAGE and transferred onto PVDF membranes (Bio-Rad, #1704274). Membranes were blocked in QuickBlock Blocking Buffer (Beyotime, #P0252) at room temperature for 20–30 min and incubated with primary antibody at 4°C overnight. After being washed five times using PBST, the membranes were incubated with secondary antibodies at room temperature for an hour. The secondary antibodies used were goat anti-rabbit IgG-HRP (Jackson Immunoresearch, #111035003, 1:10000) and goat anti-mouse IgG-HRP secondary antibody (Jackson Immunoresearch, #115035003, 1:10000). Clarity Western ECL Substrate Kit (Bio-Rad, #1705060) and Chemidoc system (Bio-Rad, #1708370) were then used for immunoblotting.

Cell cycle analysis

Cells were trypsinized, and then fixed by 4% paraformaldehyde (Solarbio, #P1110) for 30−60 min at room temperature. After washed by PBS supplemented with 2% BSA (Sigma-Aldrich, #B2064) for 3 times, cells were stained by FxCycle Violet Stain (Invitrogen, #F10347) for 30−60 min. The cell cycle was then detected by flow cytometry (LSRFortessa, Becton Dickinson) and analyzed by FlowJo.

Clonogenic survival assay

RPE1 cells were seeded into 6-well plates (200 cells per well) and treated with cisplatin. 48 h post-treatment, cell medium was refreshed, and cells were cultured for 10−14 days. Then the plates were rinsed by PBS, fixed by methanol, and stained with 0.1% Crystal Violet (Solarbio, #G1063). The number of colonies was counted manually, and plates were imaged by Chemidoc system (Bio-Rad, #1708370).

Cell Titer Glo (CTG)

RPE1 cells were seeded into a 96-well plate (1500 cells per well) and treated with cisplatin for 48 h. Then 35 μL of CTG reagent (Promega, #G924A) was added to each well. Cells were then shaken for 2 min and incubated at room temperature for 10 min. The luminescence was then measured by microplate reader (Molecular devices).

Cell Counting Kit-8 (CCK-8)

RPE1 cells were seeded into a 96-well plate (1500 cells per well) and cisplatin was added the next day. After treated for 48 h, 10 μL of Cell Counting Kit-8 (Dojindo, #CK04) was added per well and incubated for 100 min at 37°C. The luminescence was then measured by microplate reader (Molecular devices).

Immunoprecipitation

HEK293T cells were transfected with cDNA plasmids by lipo8000 (Beyotime, #C0533). 36 h after transfection, cisplatin (4 μM) was added. 24 h post-treatment, cells were lysed in lysis buffer supplemented with protease inhibitor (Roche, #04693116001). The lysates were then incubated with ANTI-FLAG M2 Affinity Gel (Sigma-Aldrich, #A2220) or EZview Red Anti-HA Affinity Gel (Millipore, #E6779) at 4°C with rotation overnight. Then, protein-bound beads were washed by TBS 3 times and protein samples were then eluted with non-reducing SDS loading buffer (CWBIO, #CW0028) at 95°C for 10 min.

AP-MS assay

C17orf53-WT and C17orf53-K494G and empty vector plasmids carrying FLAG tag were transfected into HEK293T cells using X-tremeGENE HP DNA transfection reagent (Roche, # 06366236001). Cisplatin (4 μM) was added 36 h after transfection. After treated for 24 h, cells were prepared by immunoprecipitation with ANTI-FLAG M2 Affinity Gel (Sigma-Aldrich, #A2220) and then into

SDS-PAGE. Three replicates were conducted for each sample. The gel was stained with Coomassie blue (BBI, #A602151-0250), and total proteins of each sample were cut out of the gel. After being destained with a solution of 100 mM ammonium bicarbonate in 50% acetonitrile, the gel was reduced by dithiothreitol and alkylated by iodoacetamide. The proteins were then digested by porcine trypsin (Sequencing grade modified; Promega, Madison, WI) overnight. Then we separated the tryptic peptides and analyzed them by Thermo Orbitrap Fusion Lumos mass spectrometry. The homo sapiens Reviewed Swiss-Port database by Proteome Discoverer 2.2 software was used to align the MS data.

Apoptosis detection

Cells treated with cisplatin for 48 h were trypsinized and washed by PBS two times. Then cells were resuspended with Annexin V binding buffer and stained with Annexin V-APC/DAPI (Procell, #P-CA-248). Following incubation, cells were assessed by flow cytometry (LSRFortessa, Becton Dickinson).

CHX chase assay

HEK293T cells (4×10^5 cells per well) were seeded onto 12-well plates and transfected with plasmids encoding wild-type or mutant proteins. About 36 h post-transfection, cells were treated with 100 mg/mL of CHX. Then, cell lysates were collected at different time points and subjected to immunoblot analysis. Cells were harvested at 0, 2, 2.5, 5 and 10 h after CHX treatment. Quantification was performed using ImageJ software and normalized by vinculin level of each sample.

QUANTIFICATION AND STATISTICAL ANALYSIS

Quantification of protein abundance in immunoblotting was performed using ImageJ and normalized by controls as indicated in the corresponding figure legends. Fluorescence-activated cell sorting data were quantified using FlowJo, and normalized by controls as indicated in the corresponding figure legends. Protein-protein interaction networks were analyzed by STRING and created by Cytoscape. The p value of RNAseq analysis was calculated using the Wilcoxon test. Significance levels are indicated as $^*p < 0.05$, $^{**}p < 0.01$, $^{***}p < 0.001$, while ''NS'' denotes non-significant results.